Dalton Transactions

ROYAL SOCIETY OF CHEMISTRY

PAPER

Cite this: *Dalton Trans.*, 2020, **49**, 7373

Probing the limits of linker substitution in aluminum MOFs through water vapor sorption studies: mixed-MOFs instead of mixed-linker CAU-23 and MIL-160 materials†

Carsten Schlüsener, Dustin Nils Jordan, Mergime Xhinovci, Tobie J. Matemb Ma Ntep, Alexa Schmitz, Beatriz Giesen and Christoph Janiak *

We report a systematic study on the possibility of forming mixed-linker metal–organic frameworks (MOFs) spanning between the aluminum MOFs CAU-23 and MIL-160 with their 2,5-thiophenedicarboxylate (TDC) and 2,5-furandicarboxylate (FDC) linkers, respectively. The planned synthesis of a mixed-linker MOF, combining TDC and FDC in the framework turned out to yield a rather largely intricate mixture of CAU-23 and MIL-160. This is due to the different opening angles of 150° for TDC *versus* 120° for FDC and the concomitant *cis–trans versus cis*-only OH-bridges in the infinite secondary building unit {Al(μ-OH)(O_2C–)} chains. At the same time, the CAU-23 phase is accompanied by the polymorphic MIL-53-TDC phase with *trans*-only OH-bridges. The measurement of water vapor sorption isotherms was the method of choice to confirm the formation of mixed MOFs instead of mixed-linker phases. Thereby, the water sorption isotherms indicate the simultaneous formation of both MOF phases, albeit they do not exclude mixed-linker MOFs which may have formed at low levels of substitution. The differentiation *via* powder X-ray diffractometry (PXRD), IR-spectroscopy and nitrogen sorption was either not conclusive enough or impossible, due to similarities of the neat MOF phases. The synthesized MOF mixtures within the TDC : FDC ratios of 38 : 62 up to 82 : 18 exhibit two or three uptake steps in the water sorption isotherm, with the first two corresponding to an overlay from the individual water sorption isotherm of CAU-23 and MIL-160 and a third one from the additional MIL-53-TDC.

Received 19th March 2020,
Accepted 4th May 2020

DOI: 10.1039/d0dt01044h

rsc.li/dalton

Introduction

Metal–organic frameworks (MOFs), which consist of metal ions or metal-oxido clusters connected by bridging organic ligands ("linkers"),[1–3] are actively investigated towards potential application in *e.g.* catalysis,[4,5] sensing,[6] gas separation[7,8] and storage,[9] drug delivery,[10] cyclic water adsorption processes for heat transformation (adsorption chilling)[11–14] and water harvesting from air.[15,16] The properties of MOFs are tunable through the variation of metal ions[17] and linkers.[18–21]

A new MOF called CAU-23 [Al(OH)TDC] (CAU = Christian-Albrechts-Universität), consisting of Al^{3+} ions and 2,5-thiophenedicarboxylate (TDC) linker molecules (Scheme 1), was recently published by Lenzen *et al.* and was stated as an ideal candidate for ultra-low temperature actuated adsorption-driven chillers in thermally driven adsorption heat pumps (AHPs) with an exceptional cycling stability. The most significant advantage of CAU-23 was the applicable low driving temperature (60 °C) under the retention of high uptake capacities of 0.37 g(H_2O)/g (sorbent) and a low cooling temperature of 10 °C.[22]

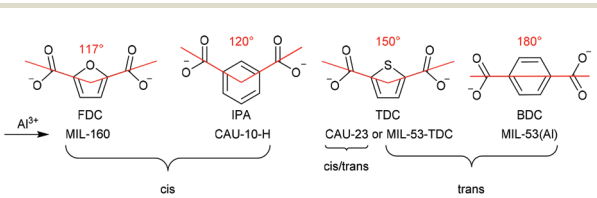

Scheme 1 Schematic illustration of linker molecules relevant in this work, their opening angles and the resulting MOFs with their *cis*- and/or *trans*-μ-OH connectivity of the AlO_6 octahedra (*cf.* Fig. 1 and Fig. S1–S4, ESI†).

Institut für Anorganische Chemie und Strukturchemie, Heinrich-Heine-Universität, D-40204 Düsseldorf, Germany. E-mail: janiak@uni-duesseldorf.de

†Electronic supplementary information (ESI) available: Brief description of cycling heat transformation with AHPs, the background of the presented MOFs, syntheses details, PXRD measurements, IR spectroscopic data, nitrogen and water sorption analyses, SEMs, TGAs and ^{1}H-NMR spectra. See DOI: 10.1039/D0DT01044H

Low-temperature cycling heat transformation with AHPs and MOFs as active materials is currently in the focus of research due to the unsurpassed tunability of MOFs as porous materials (see Scheme S1, ESI† for a short description of the working principle).[11,23–25] In comparison to the already AHP-application tested MOFs Al-fumarate (Al-FUM),[26–29] and CAU-10-H,[30,31] the new MOF CAU-23 shows a similar theoretical coefficient of performance values (COP) but exhibits a superior S-shaped water sorption isotherm.[22]

A MOF sharing the same formula unit as CAU-23, namely the polymorph MIL-53-TDC [Al(OH)TDC] (MIL = Matériaux de l'Institute Lavoisier), was reported by Tschense *et al.* and has also been investigated for potential applications other than cycling water sorption.[32–35] MIL-53-TDC also exhibits highly interesting water sorption properties with high hydrothermal stability and a favorable low isosteric heat of adsorption of only 2.6 kJ g^{-1} as this heat must be rejected to the environment and is waste heat. Furthermore, active MIL-53(Al)-TDC can be regenerated with desorption temperatures below 65 °C, with also desirable high condenser temperatures of around 40 °C and a corresponding water exchange of almost 0.35 g g^{-1}, giving a working window which renders the material an ideal candidate for adsorptive cooling applications.[32,33]

The opening angle of the TDC linker with 150° lies between the linear benzene-1,4-dicarboxylate (BDC) and V-shaped 2,5-furandicarboxylate (FDC) and 1,3-benzenedicarboxylate (isophthalate, IPA) linkers (Scheme 1). Hence, the TDC linker yielded either *trans*-connected AlO_6 in MIL-53-TDC or *cis*- and *trans*-connected AlO_6 in CAU-23 (Fig. 1, Fig. S3 and S4 in the ESI†).[22,32]

We have recently applied a solid-solution mixed-linker approach,[36] where the IPA linker in CAU-10-H was partially replaced by the FDC linker from MIL-160 (and *vice versa*) under the retention of the isoreticular structures.[37] The mixed-linker approach allowed the fine-tuning of the MOF hydrophilicity and water uptake characteristics between the limits of MIL-160 and CAU-10-H, *e.g.* by shifting the steep increase in the S-shaped water adsorption isotherm in small steps from p/p_0 = ~0.05 for MIL-160 to p/p_0 = ~0.18 for CAU-10-H. The mixed-linker materials also gave a higher coefficient of performance (COP_H) value for the obtained materials over MIL-160 under certain conditions.[37]

The term "mixed-linker" lacks a generally valid definition. MOFs with two (or more) different linker molecules in the framework can be called mixed-linker MOFs. Here we want to differentiate the non-stoichiometric substitution of similar linkers in isostructural MOFs from the stoichiometric linker composition in pillar-layered MOFs. Herein we refer to mixed-linker MOFs as materials, which are synthesized in a direct synthesis with at least two differing linker molecules that possess the same coordinating groups and connectivity and form isostructural MOFs when applied in a single-linker synthesis (isostructural mixed-linker approach).[38] Such mixed-linker MOFs have also been termed MIXMOFs, multivariate MOFs (MTV-MOFs) and mixed-component MOFs (MC-MOFs)[36,39] and were recently applied for other MOF property tunings in *e.g.* gas adsorption,[40] catalysis,[41]

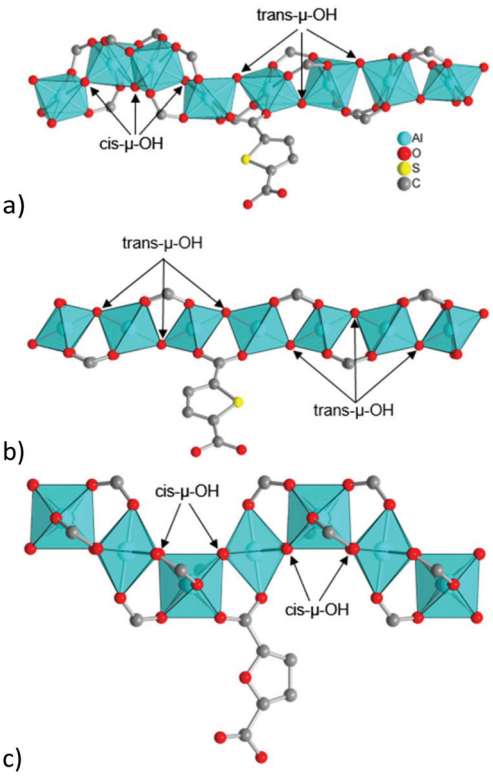

Fig. 1 Illustration of Al–O chains of (a) CAU-23 (*cis* and *trans*; helical and straight), (b) MIL-53-TDC (*trans*; straight) and (c) MIL-160 (*cis*; helical). Graphics produced by software Diamond[65] from cif-files with CSD-Refcodes ZOVHUQ (CAU-23), PIBZOS (MIL-160) and a cif file provided by Serre and co-workers for MIL-53-TDC.[22,66]

luminescence[42,43] and thermal expansion.[44] In general, mixed-linker MOFs with a random and statistical linker distribution throughout the whole framework are desired. However, the generation of such a random distribution is not straightforward for all linker combinations, due to possible core–shell composites, linker domains within the framework and transitions between these heterogeneous linker distribution arrangements. Even the formation of a MOF structure with a parent framework and the incorporation of the second linker at only specific lattice sites can occur. Also, the formation of physical mixtures of single-linker MOFs is possible and has to be ruled out.[38]

Mixed-linker MOFs are most often synthesized for isostructural single-linker parent MOFs and by employing the linker in a nonfunctionalized and a functionalized version (*e.g.* terephthalate and functionalized with –I, –Br, $–CH_3$, $–NH_3$ and –OH).[38,45] The direct synthesis of mixed-linker MOFs may seem to be the easiest method, employing all linkers and the chosen metal precursor in a conventional MOF synthesis. However, the disadvantage of the direct synthesis type is the poor product control and an unpredictable linker-ratio outcome. Even the reproducibility of the synthesis and a reliable linker-ratio characterization can be challenging.[38] The synthesis of a core–shell type MOF-5 reported is a good example, where different metal–linker solubility properties pre-

vented the random distribution of both linker types throughout the framework. The crystallization rates of the employed BDC and 2-hydroxybenzene-1,4-dicarboxylate (BDC-OH) led to the formation of a BDC rich core, acting as seeding crystals for the formation of BDC-OH rich shells.[46]

For Al-based MOFs, we are only aware that nonfunctionalized and functionalized versions of the same linker were employed, *e.g.* in the synthesis of mixed-linker MOFs of CAU-10[47–49] and MIL-53.[41,50–52]

CAU-23 and MIL-160 are seen as two of the most promising adsorbents for heat transformation. Both offer relatively high uptake values for water vapor (CAU-23:[22] 375 mg g^{-1}, 0.33p/p_0, 298 K; MIL-160:[53] 360 mg g^{-1}, 0.50p/p_0, 303 K) and exhibit favorable S-shaped isotherms with a steep rise in a small relative pressure range.[22,53–55] The beginning of water uptake for CAU-23 starts around p/p_0 = 0.25 and for MIL-160 at p/p_0 = 0.05.[22,53] The pronounced difference is based on the different hydrophilicities of the respective linker molecule and the different pore structures. For application in AHPs, MOFs should have high water vapor uptake values in the range of 0.05–0.40p/p_0.[31]

Following our mixed IPA/FDC–linker results, we chose TDC and FDC, that is CAU-23 and MIL-160 with an even higher difference of 0.25–0.05p/p_0 in the beginning of water vapor uptake compared to CAU-10-H and MIL-160 (difference 0.18–0.05p/p_0) to modulate or fine-tune the sorption properties for AHP.

Experimental

Materials and methods

All chemicals were commercially obtained from various sources and used as received without further purification. The chemicals were 2,5-furandicarboxylic acid (H_2FDC; Ox Chem: 98%, 95%; Apollo Scientific: 97%), 2,5-thiophenedicarboxylic acid (H_2TDC; Sigma Aldrich: 99%), $Al(OH)(CH_3COO)_2$ (Alfa Aesar: not specified), $AlCl_3{\cdot}6H_2O$ (Janssen Chimica: 99%), $NaAlO_2$ (VWR Chemicals: 50–56% based on Al_2O_3), NaOH (microgranules; Chem Solute: >98.8%) and NaOH (pellets; Merck: 99%). The used water was de-ionized *via* ion exchange.

Powder X-ray diffractograms (PXRD). Powder X-ray diffractograms (PXRD) were obtained at ambient temperature on a Bruker D2 Phaser (300 W, 30 kV, 10 mA; Bruker. Billerica, USA) using Cu-Kα radiation (λ = 1.54182 Å) between 5° < 2Θ < 50° with a scanning rate of 0.135° s^{-1} or 0.025° s^{-1}. The diffractograms were obtained on a flat "low background sample holder", in which at a low angle the beam spot is strongly broadened so that only a fraction of the reflected radiation reaches the detector, hence the low relative intensities measured at 2Θ < 7°. The analyses of the diffractograms were carried out with the "Match! 3.5.3.109" software.

Nitrogen (purity 99.9990%) physisorption isotherms. Nitrogen (purity 99.9990%) physisorption isotherms were obtained on a Nova 4200e or Autosorb-6 from Quantachrome at 77 K.

Water vapor sorption isotherms. Water vapor sorption isotherms were measured volumetrically on a Quantachrome VSTARTM vapor sorption analyzer with four parallel stations at 293 K. Before each sorption measurement, the samples were activated under vacuum (1×10^{-3} mbar) at 423 K for 2 h or until a pressure of 5×10^{-2} mbar was achieved.

Brunauer–Emmett–Teller (BET) surface areas. Brunauer–Emmett–Teller (BET) surface areas were calculated from four or five adsorption points in the pressure range p/p_0 = 0.006–0.08 by applying Rouquerol plots (r > 0.998), unless otherwise stated. The total pore volumes were calculated from the N_2 sorption isotherms at p/p_0 = 0.90. Density functional theory (DFT) calculations for the pore size distribution curves were done with the native NovaWin 11.03 software using the 'N_2 at 77 K on carbon, slit pore, non-local density functional theory (NLDFT) equilibrium' model for nitrogen. The Brunauer–Emmett–Teller (BET) surface areas for microporous materials with Type I isotherms should be determined and designated as 'apparent S(BET)' as 'the BET-area derived from a Type I isotherm must not be treated as a realistic probe accessible surface area' but represents an apparent surface area, which may be regarded as a useful adsorbent "fingerprint".[56] In the following, we refer to 'BET' for simplicity but imply 'apparent BET'.

Scanning electron microscopy (SEM) images. Scanning electron microscopy (SEM) images were obtained by using a Jeol JSM-6510LV QSEM advanced electron microscope (Jeol, Akishima, Japan) with a LaB6 cathode at 5–20 keV. The microscope was equipped with a Bruker Xflash 410 silicon drift detector.

Thermogravimetric analyses (TGA). Thermogravimetric analyses (TGA) were carried out on a Netzsch TG209 F3 Tarsus (Netzsch, Selb, Germany) device under a synthetic air atmosphere, ramping at 5 K min^{-1} to 650 °C.

FT-IR spectra. FT-IR spectra were measured in ATR-mode (Platinum ATR-QL, Diamond) on a Bruker TENSOR 37 IR spectrometer in the range of 4000–550 cm^{-1}.

Elemental (CHN) analyses. Elemental (CHN) analyses were performed on a PerkinElmer CHN 2400 analyzer (PerkinElmer, Waltham, USA).

^{1}H-NMR spectra. ^{1}H-NMR spectra were recorded on Bruker Avance III – 300 (^{1}H: 300 MHz) and 600 (^{1}H: 600 MHz) instruments. Approximately 10–20 mg of each MOF sample was dissolved in 5% NaOD in D_2O.

High-angle annular dark-field scanning transmission electron microscopy (HAADF-STEM). High-angle annular dark-field scanning transmission electron microscopy (HAADF-STEM) imaging was performed on a FEI Tecnai G2 F20 electron microscope (Gemeinschaftslabor für Elektronenmikroskopie RWTH-Aachen, Ernst Ruska-Centrum für Mikroskopie und Spektroskopie mit Elektronen, Jülich)[57] operating at 200 kV accelerating voltage and equipped with a Gatan UltraScan 1000P detector. The MOF-sample was dispersed in acetonitrile and one drop of the dispersion was placed on a 200 μm carbon-coated copper grid and dried under air.

EDX spectroscopy and elemental mapping acquired in STEM mode were also performed on an FEI Tecnai G2 F20. For point EDX measurements, the exposure time of the individual EDX spectrum was 3 min. All STEM measurements were carried out using the Gatan Digital Micrograph software.

Syntheses of MOF materials

Lenzen *et al.* reported the green synthesis route for CAU-23 with a relatively large scale approach using 4.3 g 2,5-thiophenedicarboxylic acid (H_2TDC; 25 mmol), 2.0 g sodium hydroxide (NaOH; 50 mmol), two aqueous solutions of aluminum chloride ($AlCl_3{\cdot}6H_2O$;18.75 mL; 1.0 mol L^{-1}; 18.75 mmol) and sodium aluminate ($NaAlO_2{\cdot}0.2H_2O$; 12.5 mL; 0.5 mol L^{-1}; 6.25 mmol) and 100 mL of distilled water.[22] Here we followed a modified protocol of Lenzen *et al.*,[22] with reduced batch sizes, for example, only one-fourth of the reported molar amounts were used.

CAU-23. H_2TDC (6.26 mmol) was mixed with 12.75 mmol of NaOH and stirred in 25 mL de-ionized H_2O until a clear solution of Na_2TDC was achieved. After complete dissolution of H_2TDC, 1 eq. of Al^{3+} from two aqueous solutions of aluminum chloride hexahydrate ($AlCl_3{\cdot}6H_2O$; 1.0 mol L^{-1}; 4.69 mL; 4.69 mmol) and sodium aluminate ($NaAlO_2{\cdot}0.2H_2O$; 0.5 mol L^{-1}; 3.1 mL; 1.56 mmol) was added to the linker solution (Table S1 in the ESI†). The resulting suspension was then stirred under reflux conditions for 6 h.

The cooled down suspension was centrifuged to recover a white product. The precipitate was dispersed three times in 45 mL each of de-ionized water and afterwards centrifuged. In a final step, the product was dispersed in 45 mL de-ionized water and stirred for at least 16 h before being centrifuged again. The resulting white solid was dried in a vacuum oven at 60 °C (*ca.* 10 mbar) for not less than 24 h. The yield is listed in Table S1 in the ESI.†

We further investigated the synthesis of CAU-23 with varying synthesis conditions (*e.g.* reaction scale, reaction time and washing procedure). We note that we could only reproduce CAU-23, despite various attempts, with a BET-surface area of at best 1056 $m^2\ g^{-1}$ compared to the literature value of 1250 $m^2\ g^{-1}$ reported by Lenzen *et al.*[22] The introduction of small amounts of ≤5% FDC to the synthesized materials enhanced the porosity. The BET-surface areas of respective materials were comparable to the published values of CAU-23 by Lenzen *et al.*[22]

With the amount of 10% H_2FDC offered during the CAU-23 synthesis, a mixed MOF with 1 mol% of FDC or a molar TF ratio of 99 : 01 was obtained, which matched the CAU-23 porosity characteristics. The BET-surface area and total pore volume of TF 99 : 01 were comparable to the published values of CAU-23 by Lenzen *et al.*[22] Hence, in the following water and gas sorption studies, CAU-23 synthesized in this work is a material with a TF ratio of 99 : 01, unless otherwise noted.

MIL-160. The synthesis was carried out as described for CAU-23 with 6.25 mmol H_2FDC. The yield is listed in Table S1, ESI.†

MIL-53-TDC. The synthesis of MIL-53-TDC was performed following a protocol of Tannert *et al.*, albeit with lower amounts of the starting materials.[33] H_2TDC (0.270 g, 1.57 mmol) was dissolved in 2.5 mL DMF and a solution of 1.19 g (1.79 mmol) aluminum sulfate octadecahydrate ($Al_2(SO_4)_3{\cdot}18H_2O$) in 10 mL de-ionized water was added. The resulting suspension was then stirred under reflux conditions at 135 °C for 24 h (Table S3 in the ESI†). The workup was as described for CAU-23. The yield is listed in Table S3, ESI.†

Mixed materials. For mixed 2,5-thiophenedicarboxylate/2,5-furandicarboxylate (TF) MOF materials, different amounts of H_2TDC and H_2FDC (taken together as 1 eq.; typically, 1.57 mmol) were mixed with 2 eq. of NaOH and stirred in 10 mL de-ionized H_2O until a clear solution of Na_2TDC and Na_2FDC was achieved. After complete dissolution of H_2TDC and H_2FDC, 1 eq. of Al^{3+} from two aqueous solutions of aluminum chloride hexahydrate ($AlCl_3{\cdot}6H_2O$; 1.17 mL of 1 mol L^{-1} storage solution) and sodium aluminate (($NaAlO_2{\cdot}0.2H_2O$; 0.78 mL of 0.5 mol L^{-1} storage solution) was added to the linker solution. The specific molar amounts are given in Table S1 in the ESI.† The resulting suspension was then stirred under reflux conditions for 24 h. We note that the extended reaction time for mixed MOFs over the 6 h given for neat CAU-23 and MIL-160 led to a higher crystallinity and porosity. The workup was as described before. The yield is listed in Table S1, ESI.†

Materials synthesized with both linkers (TDC and FDC) are designated as TF xx : yy (T = TDC, F = FDC; xx = molar fraction of TDC, yy = molar fraction of FDC). The molar fractions of TDC and FDC were determined postsynthetically by digestion NMR in 5% NaOD in D_2O (see ^{1}H NMR spectra in section S10, ESI† for details).

Results and discussion

From the at first sight apparent near identity of 2,5-thiophenedicarboxylate (TDC) and 2,5-furandicarboxylate (FDC), the synthesis of mixed-ligand aluminum MOFs stretching from the single-linker MOF CAU-23 (TDC only) to MIL-160 (FDC only) seemed straightforward in order to fine-tune the hydrophilicity.

TDC as a V-shaped linker with an opening angle of 150° lies directly in between typical V-shaped (*e.g.* FDC, 117°; isophthalate, IPA 120°) and linear linkers (*e.g.* terephthalate, BDC, 180°; fumarate, FUM, 180°) (Scheme 1). Whether the linker TDC would lead to a combined *cis–trans*-connected MOF as in CAU-23 was uncertain at the beginning. With the discovery of MIL-53-TDC, a *trans*-only-connected phase was described.[32] Likewise, a *cis*-only-connected structure of TDC with Al^{3+} may also be possible.

Aside from the stereochemistry, the MOFs CAU-23 and MIL-160 have the same infinite secondary building units (SBU) of formula $\{Al(OH)(O_2C\text{-})_2\}$, composed of corner-sharing $\{Al(OH)_2(O\text{–}C\text{–}O)_4\}$ octahedra. The difference lies "only" in the combined *cis*- and *trans*- (CAU-23) or solely *cis*-positioning

(MIL-160) of the bridging μ-OH-vertices. The structure of CAU-23 consists of alternating units of four consecutive *cis*- and four *trans*-corner-sharing $\{Al(OH)_2(O–C–O)_4\}$ polyhedra in the infinite SBU. These different sections resemble a combination of MIL-160 (*cis*) and MIL-53-TDC (*trans*). It did not seem impossible that the *cis*-sections could be bridged by the FDC ligand and the *trans*-sections by the TDC ligand to arrive at a mixed-linker MOF.

Nine materials with varying fractions of TDC and FDC and the three single-linker MOFs CAU-23, MIL-53-TDC and MIL-160 were synthesized (Scheme 1). Different amounts of H_2TDC and H_2FDC were dissolved under complete deprotonation with NaOH in water. Aqueous solutions of $AlCl_3{\cdot}6\ H_2O$ and $NaAlO_2$ were consecutively added to the linker solution and the reaction mixture was refluxed for 24 h. CAU-23,[22] MIL-160 [53,58] and MIL-53-TDC[33] were obtained from the modified literature procedures (for further synthesis details, see the Exp. section, Scheme 2 and Section S3 in the ESI†).

The mixed materials are denoted as TF xx : yy (T = TDC, F = FDC; xx = fraction of TDC, and yy = fraction of FDC). The values for the MOF-incorporated fractions of TDC and FDC were confirmed post-synthetically through solution ^{1}H NMR-spectroscopy with the MOFs dissolved in 5% NaOD in D_2O (see ^{1}H NMR spectra in section S10 in the ESI† for details). Based on the integral ratios of TDC and FDC protons in the ^{1}H NMR spectra, the actual linker ratios were calculated (see Table S1 in the ESI†). The molar starting and the postsynthetically determined ligand ratio were within a few percent for synthesis ratios of T : F ≤ 0.5 : 0.5. For synthesis ratios of T : F ≥ 0.6 : 0.4, up to 20% more TDC than offered was found in the mixed materials with reciprocally less FDC (Table S1, ESI†). CHNS-elemental analyses support the post-synthetic NMR determination and show a consistent decrease in sulfur content with a decreasing fraction of TDC (when starting from CAU-23) (Table S2, ESI†).

All materials were obtained as highly microcrystalline powders. Powder X-ray diffraction (PXRD) patterns of all MOF products are shown in Fig. 2. The diffractograms of the single-linker MOFs match their respective simulated diffractograms. Deviations in the relative intensities of the reflections between the simulated and experimental diffractograms are due to the used flat-surface sample holder (for further details see the Experimental section).[22,58] Characteristic reflections at 17.1 and 17.4°2 theta for CAU-23 (space group $P2_12_12$) and at 15.3 and 22.8°2 theta for MIL-160 (space group $I4_1md$) allow the differentiation of each of the two MOFs. The characteristic reflections of CAU-23 and MIL-160 can also be observed in the intended mixed-linker materials. In these mixed materials, the reflection intensities for CAU-23 and MIL-160 vary depending on the respective linker fractions.

A possible MIL-53-TDC phase cannot be ruled out, due to the smaller number of reflections for MIL-53-TDC (space group *Pmna*) which in addition overlap with CAU-23. Overall, the PXRD gives a first indication that it is not mixed-linker MOFs which are formed but a mixed-MOF material of CAU-23/MIL-53-TDC with MIL-160. For mixed-linker MOFs, one would expect a single phase as determined by the higher linker fraction.

To the best of our knowledge, the aspect of mixed-linker *versus* mixed-MOFs has not been elucidated before for structurally very similar MOFs where the PXRD patterns do not allow for a distinction.

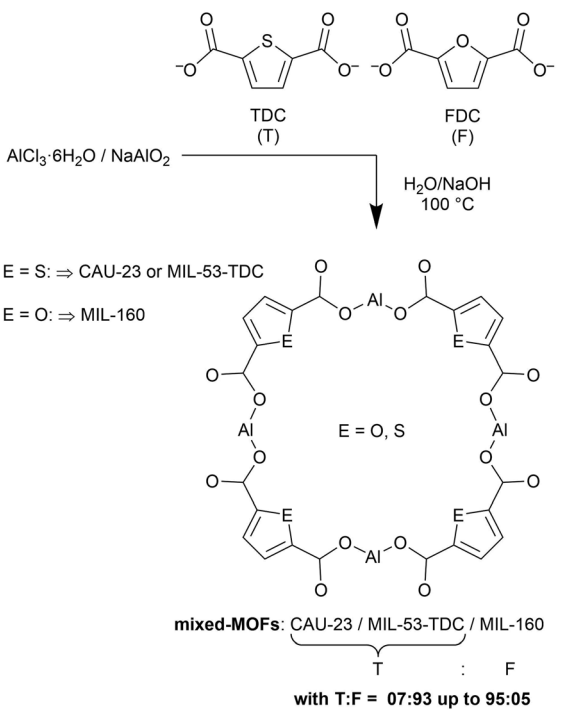

Scheme 2 Schematic formation of the MOF materials with varying fractions of TDC and FDC. The given ratio 2,5-thiophene- to 2,5-furandicarboxylate (T : F) was determined postsynthetically by digestion NMR.

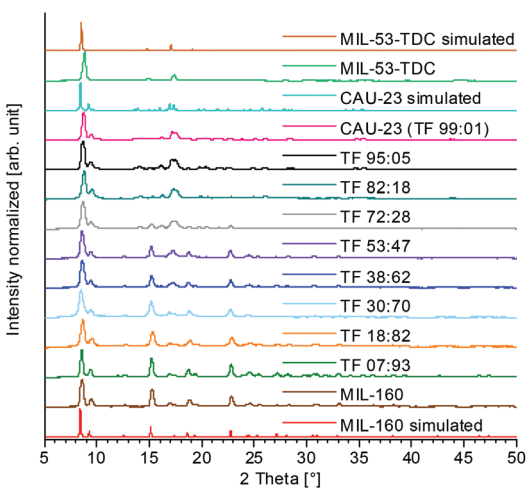

Fig. 2 PXRD patterns of mixed TF materials CAU-23, MIL-53-TDC and MIL-160 together with simulated diffractograms of CAU-23, MIL-53-TDC and MIL-160. The theoretical powder patterns were calculated from the CSD-deposited cif-files of CAU-23 (CSD-Refcode ZOVHUQ[22]), MIL-160 (CSD-Refcode PIBZOS[66]) and MIL-53-TDC from a cif-file that was generously provided by Serre and co-workers. For an enlarged version of the figure with a full-page width see Fig. S5, ESI.†

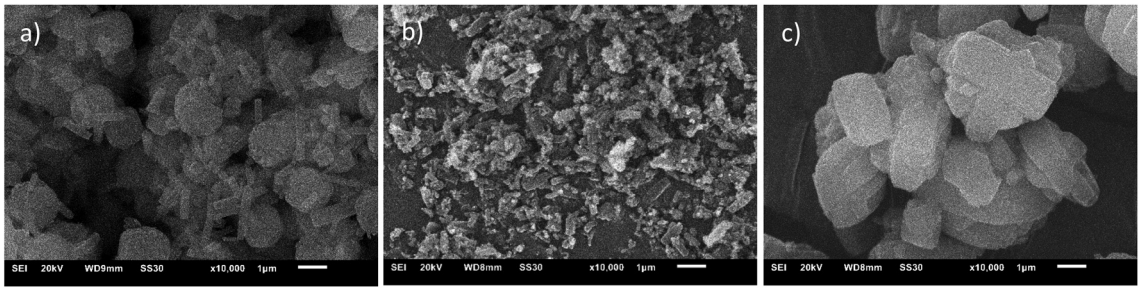

Fig. 3 SEM images of (a) CAU-23 (TF 99 : 01), (b) TF 53 : 47, (c) MIL-160. Magnification in all images is 10 000; the scale bar is 1 μm; see section S10 in the ESI† for additional SEM images.

Selected scanning electron microscopy (SEM) images indicate that the obtained materials have no characteristic microcrystal morphology and show a tendency to form particle agglomerates (Fig. 3 and Section S8, ESI†). Microcrystallinity can partially be recognized by the facetted primary particles. The mixed-MOF materials show varying particle and agglomerate sizes, and in some cases rod-like and smaller spherical agglomerated particles were observed. The occurrence of two different morphologies is another indicator for the formation of two different phases next to each other in a mixed-MOF instead of the intended mixed-linker material.

Thermogravimetric (TG) analysis measurements under a synthetic air atmosphere to a final temperature of 650 °C show for most samples a two-step weight loss (Fig. 4 and Section S9, ESI†). From 25 °C to 200 °C adsorbed H_2O molecules are removed. The second weight loss starts around 350 °C and is related to the decomposition of the linkers. Above 500 °C, the framework is decomposed and the residual amorphous mass consists of an undefined mixture of Al_2O_3 and Al_2O_2S.

Sorption properties

The Brunauer–Emmett–Teller, BET, surface areas were determined for all synthesized materials from N_2 sorption isotherms at 77 K. All mixed materials have high BET-surface areas between 834–1272 $m^2\ g^{-1}$, which have to be compared with the single-linker BET-surface areas for CAU-23 of 1250 $m^2\ g^{-1}$ [22] and MIL-160 1162 $m^2\ g^{-1}$ (Lit.:[53,58] 1070–1150 $m^2\ g^{-1}$).

Compared to the surface areas of the single-linker MOFs CAU-23 and MIL-160, the mixed-MOF BET-surfaces and pore volumes mostly lie somewhat under the calculated values based on the linker fractions (Fig. 5 and Table 1) but are still within the experimental error range of ± 40 $m^2\ g^{-1}$ for S(BET) and ± 80 $m^2\ g^{-1}$ for $S(BET)_{calc}$ (see footnote a in Table 1) as

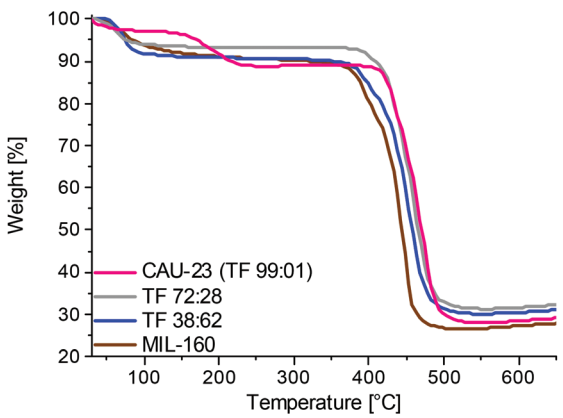

Fig. 4 Selected TGA curves of single-linker MOFs CAU-23 (TF 99 : 01) and MIL-160 and selected mixed MOFs TF 72 : 28 and TF 38 : 62 under a synthetic air atmosphere, and heating rate 5 K min^{-1}. See section S9 in the ESI† for additional details.

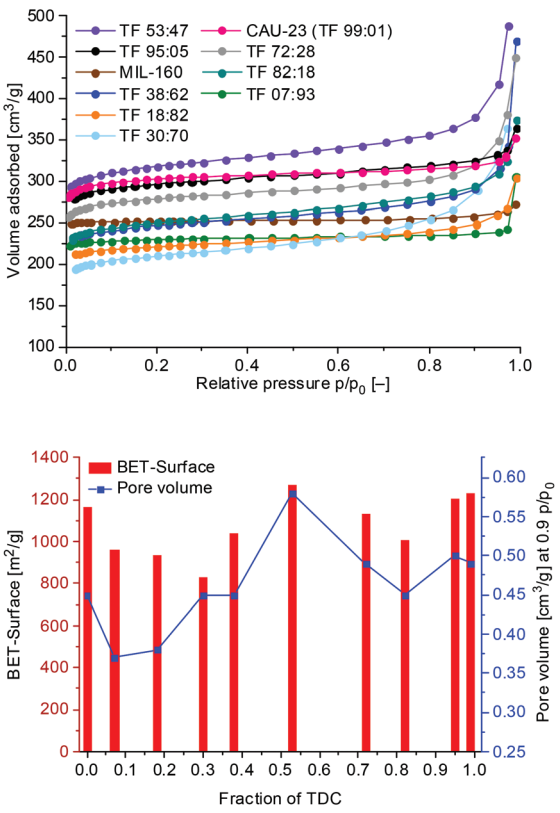

Fig. 5 Top: N_2 adsorption isotherms of mixed MOFs with different ratios of linker fractions. For clarity, only the adsorption isotherms are shown. See Fig. S8, ESI† for full N_2 sorption isotherms (including desorption branches). Bottom: Results of mixed MOF materials: BET-surface areas and pore volumes.

Table 1 Results of N_2 sorption of TF materials

Compound	$S(BET)^a$ [$m^2\ g^{-1}$]	$S(BET)_{calc.}{}^a$ [$m^2\ g^{-1}$]	% of calc. $S(BET)$ [%]	$V_{pore(total)}{}^b$ [$cm^3\ g^{-1}$]	Calc. $V_{pore(total)}{}^{b,c}$ [$cm^3\ g^{-1}$]	% of calc. $V_{pore(total)}$ [%]	$V_{pore\ (micro;NLDFT)}{}^d$ [$cm^3\ g^{-1}$]	$V_{pore(micro)}{}^e$ [$cm^3\ g^{-1}$]	$V_{total} - V_{micro}{}^f$ [$cm^3\ g^{-1}$]	$V_{total} - V_{micro}{}^g$ [$cm^3\ g^{-1}$]
CAU-23 Lit.[22]	1250	—	—		—	—	0.48[i]	—		
CAU-23 (TF 99 : 01)	1232	1231	100	0.49	0.49	100	0.46	0.43	0.03	0.06
TF 95 : 05	1203	1229	98	0.50	0.49	102	0.45	0.42	0.05	0.08
TF 82 : 18	1005	1219	82	0.45	0.48	93	0.38	0.33	0.07	0.12
TF 72 : 28	1129	1212	93	0.49	0.48	102	0.42	0.40	0.07	0.09
TF 53 : 47	1272	1199	106	0.58	0.47	123	0.48	0.44	0.10	0.14
TF 38 : 62	1040	1189	87	0.45	0.47	97	0.37	0.34	0.08	0.11
TF 30 : 70	830	1180	70	0.45	0.46	98	0.32	0.28	0.13	0.17
TF 18 : 82	934[h]	1175	80	0.38	0.46	83	0.34	0.32	0.04	0.06
TF 07 : 93	964	1167	83	0.37	0.45	82	0.35	0.34	0.02	0.03
MIL-160	1162[h]	1162	100	0.45	0.45	100	0.43	0.41	0.02	0.04
MIL-160 Lit.[53,58]	1070–1150	—	—		—	—	0.40–0.48[j]			
MIL-53-TDC	1029[i]	—	—	0.44	—	—	0.39	0.36		
MIL-53-TDC Lit.[32,33]	1150–1102	—	—	0.48[k]–0.46	—	—	—	—		

[a] From the repeated (up to four times) N_2 sorption studies with BET-surface area determination of samples from the same batch we can note that the deviation of surface area is ± 40 $m^2\ g^{-1}$ in the range of 1000–1200 $m^2\ g^{-1}$ or about 4%. In $S(BET)_{calc}$ two fractional surface areas are added, doubling the error to ± 80 $m^2\ g^{-1}$ (~8%). S(BET) is calculated as the sum of the linker-fraction-weighted surface areas of the neat MOFs (CAU-23 = 1232 $m^2\ g^{-1}$; MIL-160 = 1162 $m^2\ g^{-1}$) from the following formula $S(BET)_{calc}$ = Fraction(TDC) × 1232 $m^2\ g^{-1}$ + Fraction(FDC) × 1162 $m^2\ g^{-1}$. [b] Total pore volume ($V_{pore(total)}$) at p/p_0 = 0.90 for pores ≤20 nm. From the repeated (up to four times) N_2 sorption studies with V_{pore} determination of samples from the same batch, we can note that the deviation in V_{pore} is ± 0.02 $cm^3\ g^{-1}$ in the range of 0.50 $cm^3\ g^{-1}$. In calc V_{pore} two fractional surface areas are added, doubling the error to ± 0.04 $cm^3\ g^{-1}$. [c] Calc $V_{pore(total)}$ calculated as the sum of the linker-fraction-weighted pore volumes of the neat MOFs (CAU-23 = 0.49 $cm^3\ g^{-1}$; MIL-160 = 0.45 $cm^3\ g^{-1}$) from the following formula calc. $V_{pore(total)}$ = Fraction(TDC) × 0.49 $cm^3\ g^{-1}$ + Fraction(FDC) × 0.45 $cm^3\ g^{-1}$. [d] Micropore volume ($V_{pore(micro;NLDFT)}$) calculated from the N_2 adsorption isotherm at p/p_0 = 0.1 for pores with $d \leq$ 2 nm (20 Å). [e] Micropore volume ($V_{pore(micro)}$) refers to the volume that originates only from micropores, obtained by the *V*–*t*-method with the thickness method 'DeBoer' in the range of $0.15 < p/p_0 < 0.55$. All correlation coefficients (r) within calculations were ≥0.998. [f] Difference of $V_{pore(total)}$ and $V_{pore(micro;NLDFT)}$. [g] Difference of $V_{pore(total)}$ and $V_{pore(micro)}$ by the *V*–*t*-method. [h] Only a 2-point BET with a positive *C*-constant possible. [i] Only a 3-point BET with a positive *C*-constant possible. [j] Micropore volume with undisclosed conditions. [k] Micropore volume determined at p/p_0 = 0.5.

well as ± 0.02 $cm^3\ g^{-1}$ for V_{pore} and ± 0.04 $cm^3\ g^{-1}$ for calc V_{pore} (see footnote b in Table 1). A noteworthily different sample is TF 53 : 47 with a higher surface area than its neighboring TF samples and especially a high total pore volume of 0.58 $cm^3\ g^{-1}$, which is much higher than the total pore volume of CAU-23 (0.49 $cm^3\ g^{-1}$) and MIL-160 (0.45 $cm^3\ g^{-1}$) and consequently significantly exceeds the calculated pore volume (Table 1). At the same time, the micropore volume of TF 53 : 47 is only slightly higher than those of the parent MOFs, which indicates a sizable fraction of additional mesopores. A closer inspection of total and micropore volume also reveals that this increased mesopore volume is found from about TF 82 : 18 to TF 30 : 70. The partial mesoporosity is also reflected in the hysteresis of the N_2 sorption isotherms (Fig. S8, ESI†).

We note that the N_2 sorption isotherms, BET surface area and porosity do not indicate if a mixed-linker or mixed-MOF material has been formed. Nitrogen sorption isotherms only reflect and yield the changes in porosity, but water vapor sorption isotherms should be able to assess the aspect of mixed-linker[37] *versus* mixed-MOF material. MOFs are typically less hydrophilic than zeolites and feature S-shaped Type V sorption isotherms for water with a steep increase at higher p/p_0.[14,56] For MOFs with one type of pore structure there will be a single step in this S-shaped isotherm. For mixed-linker MOFs the steep increase should gradually shift with the linker ratio between the steep increase of the two single-linker parent MOFs.[37] For mixed-MOF materials, the water sorption isotherm should be a superposition of the individual isotherms weighted by the linker fraction.

The water sorption isotherms in Fig. 6 show that mixed materials with a larger excess of one linker exhibit S-shaped isotherms with the steep increase similar to the single-linker MOFs (see Section S7, ESI† for an explanation of the S-shape). Thus, a CAU-23 type isotherm with the increase at ~$0.25p/p_0$ is obtained for TF 82 : 18 and 95 : 05 (Fig. 6a), whereas a MIL-160 type isotherm with the increase at ~$0.05p/p_0$ is given by TF 07 : 93, TF 18 : 82 and TF 30 : 70 (Fig. 6c). The uptake amount is modulated in line with the pore volume (Fig. 7). Mixed materials with fractions from TF 72 : 28 to TF 38 : 62 exhibit water isotherms with uptake steps at ~$0.05p/p_0$ and ~$0.25p/p_0$, which are evidently a superposition of the isotherms of the single-linker MOFs MIL-160 and CAU-23 (Fig. 6b). The water sorption isotherms of these mixed materials, thus, correspond to a physical *ex situ* mixture of the corresponding amounts of CAU-23 and MIL-160 (Fig. S10, ESI†).

For materials with a predominant major phase and the minor phase below ~30 wt% as shown in Fig. 6a and c, the water uptake behavior can be dominated by the major phase

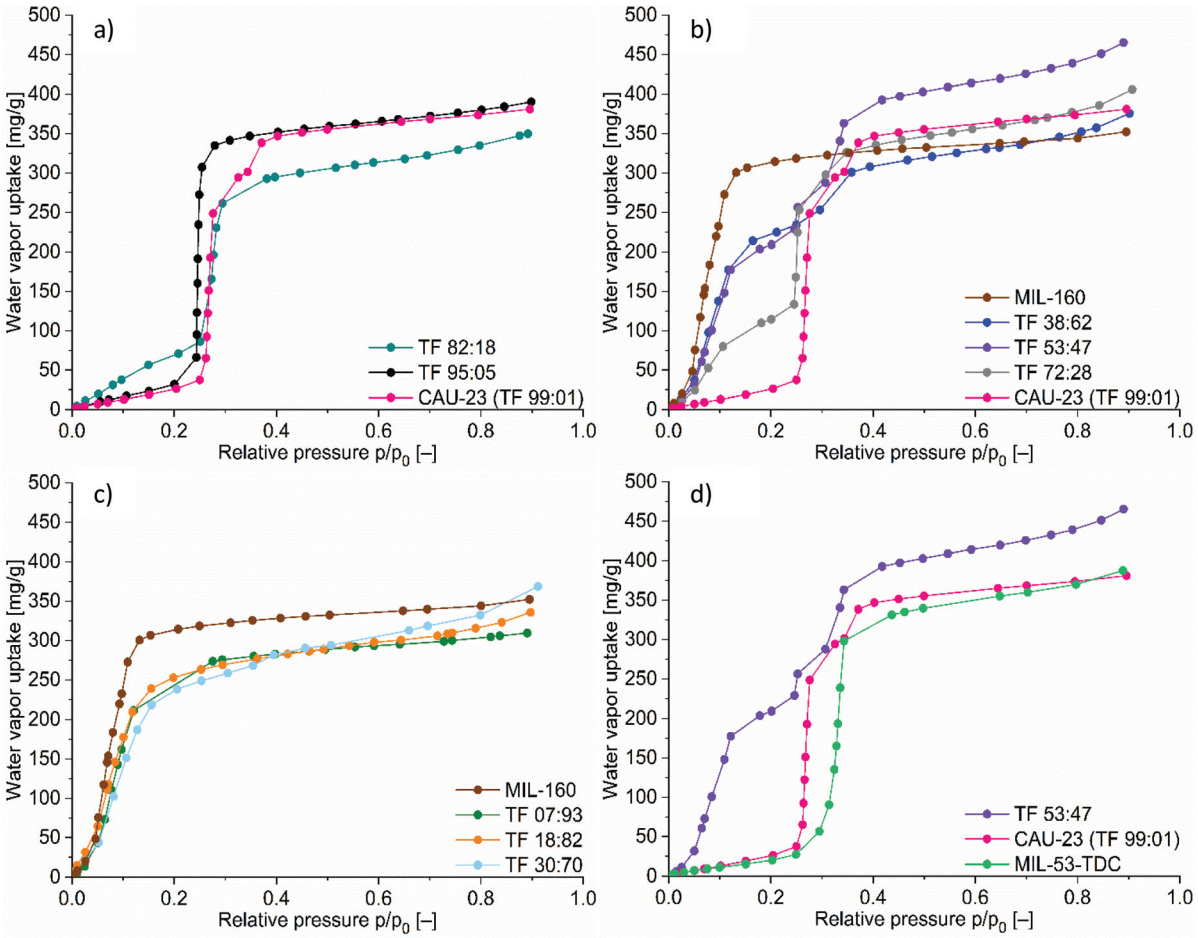

Fig. 6 Water vapor adsorption isotherms at 293 K for mixed TF-MOFs and single-linker MOFs (MIL-160 and MIL-53-TDC). (a) Excess of TDC. (b) Nearly equal amounts of both linkers. (c) Excess of FDC. (d) CAU-23 and MIL-53-TDC comparison. For clarity, only the adsorption isotherm parts are depicted. See section S7, ESI† for full water vapor sorption isotherms (including desorption branches).

and the minor phase may not exhibit its footprint. This seems to be especially the case when the minor phase is the more hydrophobic one. While the more hydrophilic MIL-160 phase already shows up at ~18% in the TF 82 : 18 material with an increasing water uptake between $0.05 < p/p_0 < 0.25$ (Fig. 6a), the more hydrophobic CAU-23 phase is first seen with its step at ~$0.25p/p_0$ in the TF 38 : 62 material, that is, at ~38% contribution (Fig. 6c).

For our CAU-23(TF 99 : 01) material, we note that there is an uptake step around $0.3p/p_0$ which was not observed in the work by Lenzen *et al.*[22] Also, TF 53 : 47 with its exceptional high uptake shows a three-stepped sorption isotherm (Fig. 6d). We explain this third uptake step through the formation of a third phase, namely MIL-53-TDC, which has its uptake step at ~$0.35p/p_0$ (Fig. 7d).[32,33] MIL-53-TDC was first published by Tschense *et al.* in 2017 [32] and was evaluated in our group for heat transformation applications.[33] MIL-53-TDC, which is difficult to separately detect by PXRD, may form together with the CAU-23 phase, either through the small changes in synthesis conditions or through the admixture of the tiny amounts of FDC. The possible formation of a MIL-53-TDC phase in a purely aqueous synthesis is intriguing and has not been reported yet, and so far MIL-53-TDC has only been synthesized in a water–DMF mixture.

To the best of our knowledge, multi-stepped water sorption isotherms are unknown for the neat single-linker MOFs with an identical pore structure (*e.g.* CAU-23 and MIL-160). The MOFs MIL-101, MIL-100 and DUT-67 show several water adsorption steps, due to their pore structures with two different pore sizes (MIL-101: 29, 34 Å; MIL-100: 25, 29 Å; DUT-67: 8.8, 16.6 Å).[24,25,59–61]

We note that water vapor sorption isotherms provide an interesting means to discern phases of different hydrophilicities/~phobicities, which are otherwise structurally too similar to be differentiated by PXRD. Here we show that water sorption isotherms can unequivocally differentiate the case of mixed-MOF materials from mixed-linker MOFs. The case of mixed-MOF materials is clearly revealed if the fraction of both phases is high enough to have their distinct isotherm curvature show up in the full isotherm (Fig. 6c). Nevertheless, there is a certain probability that the introduction of both linkers in one MOF phase, *i.e.* a mixed-linker MOF may have formed at low

levels of substitution. Unfortunately, due to the high similarity of the PXRD patterns, the verification of a minor mixed-linker MOF in the presence of major mixed-MOF phases seems virtually impossible.

We ascribe the formation of a mixture of single-linker Al-MOF phases rather than mixed-linker Al-MOFs to the small but important *cis–trans* structural differences between CAU-23 and MIL-160 (Fig. 1). CAU-23 has a V-shaped linker with a relatively large opening angle (Scheme 1) and consists of alternating units of four consecutive *trans*- and four *cis*-corner-sharing AlO_6 polyhedra in the infinite SBU. The Al-MOF MIL-160 and its structural parent CAU-10-H have V-shaped linkers FDC and IPA with small opening angles of ≤120° (Scheme 1) and have both *cis*-connected AlO_6 polyhedra (Fig. S1–S4 in the ESI†). MIL-53-TDC possesses the MIL-53-type structure with an infinite SBU of entirely *trans*-connected AlO_6 polyhedra, *cis*-connected polyhedra are leading to helical chains, whereas *trans*-sharing polyhedra are forming infinite straight chains. Hence, in CAU-23 there are alternating helical and straight sections. The occurrence of two different Al–O-chain connectivities in one crystal structure is surprising and unique, as the different sections resemble a combination of either MIL-53-TDC (*trans*) and MIL-160 or CAU-10-H (*cis*) (Fig. 1 and Fig. S1–S4†).[22,58,62,63]

The opening angle between the carboxylate groups of the used linker molecule determines the *cis–trans* generated structure for Al-MOFs.[22] Linear linkers with an opening angle of 180° (*e.g.* terephthalate and fumarate) lead to *trans*-connected AlO_6 polyhedra (MIL-53 and Al-FUM). The V-shaped linker with an opening angle around 120° (FDC 116°; IPA, 120°) gives *cis*-connected AlO_6 polyhedra (MIL-160, CAU-10-H).[30,62,64,66] Due to the differing linker opening angles and resulting (*cis–trans*) SBU topologies, the side-by-side formation of both individual MOF phases seems to be clearly favored over the formation of a mixed-linker phase.

For TF 53 : 47, the high-water uptake can be understood from its increased total pore volume (Table 1 and Fig. 7). In Fig. 7, the water uptake values are plotted *versus* the pore volume. Both the water uptake values directly after the steep rise of the last uptake step *versus* micropore volume (from NLDFT; at $0.1p/p_0$) as well as the total water uptake *versus* total pore volume; both at $0.9p/p_0$ show a reasonable linear correlation.

To support the existence of different phases in the obtained TF 53 : 47 material, point EDX measurements of diffuse and rod-like particles in the STEM image (Fig. 8, *cf.* SEM images in Fig. 3b and Section S8 in the ESI†) revealed a different elemental composition regarding aluminum and sulfur content such that the more crystalline rod-like particles show a significantly higher content of aluminum compared to sulfur. The diffuse particle regions instead had an about equal aluminum to sulfur content of 55 to 45 atom%. The formula of MIL-53-TDC and CAU-23 of [Al(OH)TDC] requires one sulfur per aluminum atom, associating their phase with the diffuse particles. These findings correspond with the simultaneous formation of two MOF phases from a mixed-linker approach.

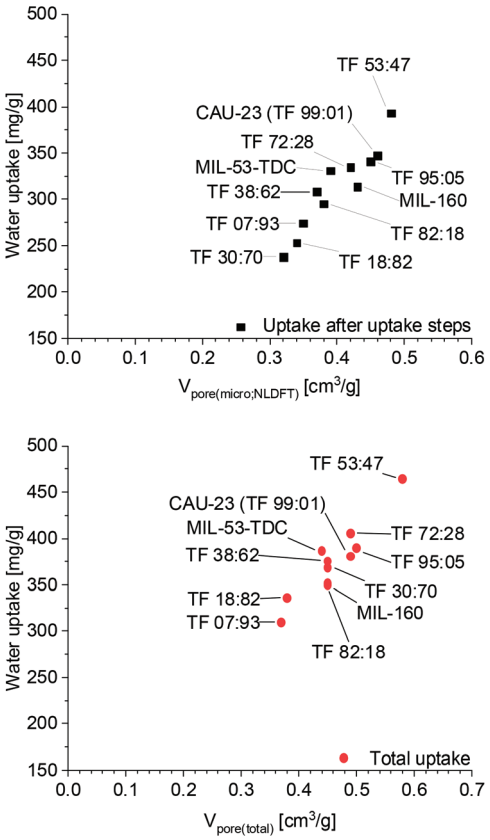

Fig. 7 Water uptake *vs.* pore volume of all materials. Top: Uptake after uptake steps *vs.* micropore volume ($(V_{pore(micro;NLDFT)}$) calculated from N_2 adsorption isotherm at p/p_0 = 0.1). Bottom: Total uptake *vs.* total pore volume ($(V_{pore(total)}$ calculated from N_2 adsorption isotherm at p/p_0 = 0.9). See Table S4, ESI† for the respective water uptake values.

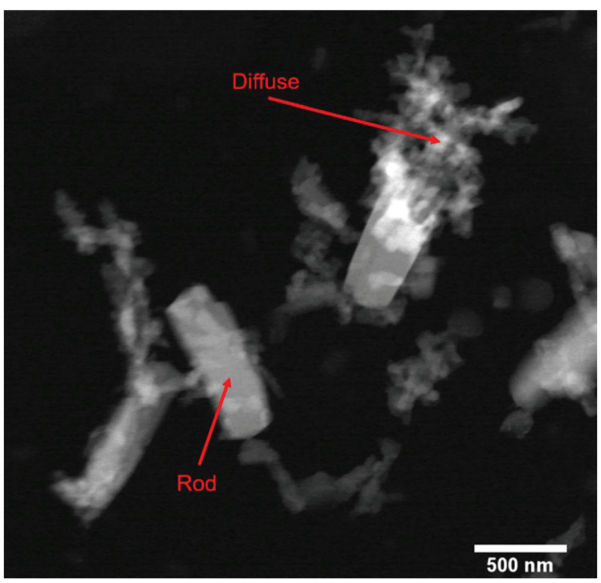

Fig. 8 STEM images of TF 53 : 47 with point EDX measurements of rod (Al 85, S 15 atom%) and diffuse particle regions (Al 55, S 45 atom%).

Conclusion

We have investigated the mixed-linker solid solution approach for the preparation of mixed-linker MOFs spanning the hydrophilicity region between the less hydrophilic single-linker CAU-23 and the more hydrophilic MIL-160. The structural differences of both MOFs, in particular the *cis* or *trans* connectivity of the infinite {Al(μ-OH)(O_2C–)} SBU prevented the formation of clearly identifiable mixed-linker MOFs. Employing nearly equal fractions of 2,5-thiophenedicarboxylate (TDC) and 2,5-furandicarboxylate (FDC) led to the formation of mixed-MOF phases rather than mixed-linker MOFs. This could only be proven from water vapor sorption experiments which turned out as the method of choice to differentiate between mixed-linker and mixed-MOF phase materials. The water sorption isotherms showed water uptake steps at 0.05 and 0.25p/p_0, which correspond to the neat parent MOFs MIL-160 and CAU-23, respectively. Thereby, the water sorption isotherms indicate the simultaneous formation of both MOF phases, albeit it does not rule out that mixed-linker MOFs may have formed at low levels of substitution. Some mixed-MOF samples even exhibited an unexpected third water uptake step after 0.30p/p_0, which could be assigned to the water vapor isotherm of MIL-53-TDC. Hence, the particular formation of a MIL-53-TDC phase, hitherto unknown from purely aqueous synthesis conditions, became evident. Furthermore, the addition of small amounts of 2,5-furandicarboxylate to the synthesis of CAU-23 improved the reproducible formation of this MOF together with its crystallinity and BET-surface area.

Conflicts of interest

There are no conflicts to declare.

Acknowledgements

The authors gratefully acknowledge the financial support from the Federal German Ministry of Education and Research (BMBF) in the project Optimat under grant no. 03SF0492C.

Notes and references

1 H.-C. Zhou, J. R. Long and O. M. Yaghi, *Chem. Rev.*, 2012, **112**, 673–674.
2 H. Furukawa, K. E. Cordova, M. O'Keeffe and O. M. Yaghi, *Science*, 2013, **341**, 1230444.
3 G. Maurin, C. Serre, A. Cooper and G. Ferey, *Chem. Soc. Rev.*, 2017, **46**, 3104–3107.
4 Y.-B. Huang, J. Liang, X.-S. Wang and R. Cao, *Chem. Soc. Rev.*, 2017, **46**, 126–157.
5 A. Herbst and C. Janiak, *CrystEngComm*, 2017, **19**, 4092–4117.
6 W. P. Lustig, S. Mukherjee, N. D. Rudd, A. V. Desai, J. Li and S. K. Ghosh, *Chem. Soc. Rev.*, 2017, **46**, 3242–3285.
7 J.-R. Li, R. J. Kuppler and H.-C. Zhou, *Chem. Soc. Rev.*, 2009, **38**, 1477–1504.
8 J. Dechnik, J. Gascon, C. J. Doonan, C. Janiak and C. J. Sumby, *Angew. Chem., Int. Ed.*, 2017, **56**, 9292–9310.
9 K. Adil, Y. Belmabkhout, R. S. Pillai, A. Cadiau, P. M. Bhatt, A. H. Assen, G. Maurin and M. Eddaoudi, *Chem. Soc. Rev.*, 2017, **46**, 3402–3430.
10 P. Horcajada, R. Gref, T. Baati, P. K. Allan, G. Maurin, P. Couvreur, G. Férey, R. E. Morris and C. Serre, *Chem. Rev.*, 2012, **112**, 1232–1268.
11 F. Jeremias, D. Fröhlich, C. Janiak and S. K. Henninger, *New J. Chem.*, 2014, **38**, 1846–1852.
12 S. Cui, M. Qin, A. Marandi, V. Steggles, S. Wang, X. Feng, F. Nouar and C. Serre, *Sci. Rep.*, 2018, **8**, 15284.
13 M. F. de Lange, K. J. F. M. Verouden, T. J. H. Vlugt, J. Gascon and F. Kapteijn, *Chem. Rev.*, 2015, **115**, 12205–12250.
14 E. Hastürk, S.-J. Ernst and C. Janiak, *Curr. Opin. Chem. Eng.*, 2019, **24**, 26–36.
15 H. Kim, S. Yang, S. R. Rao, S. Narayanan, E. A. Kapustin, H. Furukawa, A. S. Umans, O. M. Yaghi and E. N. Wang, *Science*, 2017, **356**, 430–434.
16 N. Hanikel, M. S. Prévot, F. Fathieh, E. A. Kapustin, H. Lyu, H. Wang, N. J. Diercks, T. G. Glover and O. M. Yaghi, *ACS Cent. Sci.*, 2019, **5**, 1699–1706.
17 J. Zhou, H. Li, H. Zhang, H. Li, W. Shi and P. Cheng, *Adv. Mater.*, 2015, **27**, 7072–7077.
18 F. A. Almeida Paz, J. Klinowski, S. M. F. Vilela, J. P. C. Tomé, J. A. S. Cavaleiro and J. Rocha, *Chem. Soc. Rev.*, 2012, **41**, 1088–1110.
19 R. Haldar and T. K. Maji, *CrystEngComm*, 2013, **15**, 9276–9295.
20 C. R. Wade, T. Corrales-Sanchez, T. C. Narayan and M. Dincă, *Energy Environ. Sci.*, 2013, **6**, 2172–2177.
21 A. Dhakshinamoorthy, A. M. Asiri and H. Garcia, *Catal. Sci. Technol.*, 2016, **6**, 5238–5261.
22 D. Lenzen, J. Zhao, S.-J. Ernst, M. Wahiduzzaman, A. Ken Inge, D. Fröhlich, H. Xu, H.-J. Bart, C. Janiak, S. Henninger, G. Maurin, X. Zou and N. Stock, *Nat. Commun.*, 2019, **10**, 3025.
23 C. Janiak and S. K. Henninger, *Nachr. Chem.*, 2013, **61**, 520–523.
24 J. Canivet, A. Fateeva, Y. Guo, B. Coasne and D. Farrusseng, *Chem. Soc. Rev.*, 2014, **43**, 5594–5617.
25 F. Jeremias, A. Khutia, S. K. Henninger and C. Janiak, *J. Mater. Chem.*, 2012, **22**, 10148–10151.
26 M. F. de Lange, B. L. van Velzen, C. P. Ottevanger, K. J. F. M. Verouden, L.-C. Lin, T. J. H. Vlugt, J. Gascon and F. Kapteijn, *Langmuir*, 2015, **31**, 12783–12796.
27 N. Tannert, C. Jansen, S. Nießing and C. Janiak, *Dalton Trans.*, 2019, **48**, 2967–2976.
28 S. Gökpinar, S.-J. Ernst, E. Hastürk, M. Möllers, I. El Aita, R. Wiedey, N. Tannert, S. Nießing, S. Abdpour, A. Schmitz, J. Quodbach, G. Füldner, S. K. Henninger and C. Janiak, *Ind. Eng. Chem. Res.*, 2019, **58**, 21493–21503.

29 H. Kummer, F. Jeremias, A. Warlo, G. Füldner, D. Fröhlich, C. Janiak, R. Gläser and S. K. Henninger, *Ind. Eng. Chem. Res.*, 2017, **56**, 8393–8398.

30 D. Fröhlich, E. Pantatosaki, P. D. Kolokathis, K. Markey, H. Reinsch, M. Baumgartner, M. A. van der Veen, D. E. de Vos, N. Stock, G. K. Papadopoulos, S. K. Henninger and C. Janiak, *J. Mater. Chem. A*, 2016, **4**, 11859–11869.

31 D. Fröhlich, S. K. Henninger and C. Janiak, *Dalton Trans.*, 2014, **43**, 15300–15304.

32 C. B. L. Tschense, N. Reimer, C.-W. Hsu, H. Reinsch, R. Siegel, W.-J. Chen, C.-H. Lin, A. Cadiau, C. Serre, J. Senker and N. Stock, *Z. Anorg. Allg. Chem.*, 2017, **643**, 1600–1608.

33 N. Tannert, S.-J. Ernst, C. Jansen, H.-J. Bart, S. K. Henninger and C. Janiak, *J. Mater. Chem. A*, 2018, **6**, 17706–17712.

34 M. Wahiduzzaman, N. Reimer, J.-P. Itié, N. Stock, G. Maurin and P. G. Yot, *Polyhedron*, 2018, **155**, 144–148.

35 J. A. Zárate, E. Sánchez-González, T. Jurado-Vázquez, A. Gutiérrez-Alejandre, E. González-Zamora, I. Castillo, G. Maurin and I. A. Ibarra, *Chem. Commun.*, 2019, **55**, 3049–3052.

36 A. D. Burrows, *CrystEngComm*, 2011, **13**, 3623–3642.

37 C. Schlüsener, M. Xhinovci, S.-J. Ernst, A. Schmitz, N. Tannert and C. Janiak, *Chem. Mater.*, 2019, **31**, 4051–4062.

38 J. Bitzer and W. Kleist, *Chem. – Eur. J.*, 2019, **25**, 1866–1882.

39 H. Deng, C. J. Doonan, H. Furukawa, R. B. Ferreira, J. Towne, C. B. Knobler, B. Wang and O. M. Yaghi, *Science*, 2010, **327**, 846–850.

40 G. W. Peterson, K. Au, T. M. Tovar and T. H. Epps, *Chem. Mater.*, 2019, **31**, 8459–8465.

41 S. Nießing and C. Janiak, *Mol. Catal.*, 2019, **467**, 70–77.

42 J. Cornelio, T.-Y. Zhou, A. Alkaş and S. G. Telfer, *J. Am. Chem. Soc.*, 2018, **140**, 15470–15476.

43 W. J. Newsome, S. Ayad, J. Cordova, E. W. Reinheimer, A. D. Campiglia, J. K. Harper, K. Hanson and F. J. Uribe-Romo, *J. Am. Chem. Soc.*, 2019, **141**, 11298–11303.

44 S. J. Baxter, A. Schneemann, A. D. Ready, P. Wijeratne, A. P. Wilkinson and N. C. Burtch, *J. Am. Chem. Soc.*, 2019, **141**, 12849–12854.

45 D. N. Bunck and W. R. Dichtel, *Chem. – Eur. J.*, 2013, **19**, 818–827.

46 M. Kubo, H. Hagi, A. Shimojima and T. Okubo, *Chem. – Asian J.*, 2013, **8**, 2801–2806.

47 N. Reimer, B. Bueken, S. Leubner, C. Seidler, M. Wark, D. de Vos and N. Stock, *Chem. – Eur. J.*, 2015, **21**, 12517–12524.

48 H. Reinsch, S. Waitschat and N. Stock, *Dalton Trans.*, 2013, **42**, 4840–4847.

49 S. Nandi, H. Reinsch and S. Biswas, *Microporous Mesoporous Mater.*, 2020, **293**, 109790.

50 S. Marx, W. Kleist, J. Huang, M. Maciejewski and A. Baiker, *Dalton Trans.*, 2010, **39**, 3795–3798.

51 Y. Jiang, J. Huang, S. Marx, W. Kleist, M. Hunger and A. Baiker, *J. Phys. Chem. Lett.*, 2010, **1**, 2886–2890.

52 T. Stassin, S. Waitschat, N. Heidenreich, H. Reinsch, F. Puschkell, D. Kravchenko, I. Stassen, J. van Dinter, R. Verbeke, M. Dickmann, W. Egger, I. Vankelecom, D. De Vos, R. Ameloot and N. Stock, *ChemRxiv*, 2019, DOI: 10.26434/chemrxiv.8311235.v1.

53 A. Permyakova, O. Skrylnyk, E. Courbon, M. Affram, S. Wang, U.-H. Lee, A. H. Valekar, F. Nouar, G. Mouchaham, T. Devic, G. de Weireld, J.-S. Chang, N. Steunou, M. Frère and C. Serre, *ChemSusChem*, 2017, **10**, 1419–1426.

54 F. Jeremias, D. Fröhlich, C. Janiak and S. K. Henninger, *RSC Adv.*, 2014, **4**, 24073–24082.

55 S. K. Henninger, F. Jeremias, H. Kummer and C. Janiak, *Eur. J. Inorg. Chem.*, 2012, 2625–2634.

56 M. Thommes, K. Kaneko, A. V. Neimark, J. P. Olivier, F. Rodriguez-Reinoso, J. Rouquerol and K. S. Sing, *Pure Appl. Chem.*, 2015, **87**, 1051–1069.

57 Ernst Ruska-Centre for Microscopy and Spectroscopy with Electrons, FEI Tecnai G2 F20, *Journal of large-scale research facilities JLSRF*, 2016, **2**, A77, DOI: 10.17815/jlsrf-2-138.

58 A. Cadiau, J. S. Lee, D. Damasceno Borges, P. Fabry, T. Devic, M. T. Wharmby, C. Martineau, D. Foucher, F. Taulelle, C.-H. Jun, Y. K. Hwang, N. Stock, M. F. de Lange, F. Kapteijn, J. Gascon, G. Maurin, J.-S. Chang and C. Serre, *Adv. Mater.*, 2015, **27**, 4775–4780.

59 H. Furukawa, F. Gándara, Y.-B. Zhang, J. Jiang, W. L. Queen, M. R. Hudson and O. M. Yaghi, *J. Am. Chem. Soc.*, 2014, **136**, 4369–4381.

60 G. Akiyama, R. Matsuda, H. Sato, A. Hori, M. Takata and S. Kitagawa, *Microporous Mesoporous Mater.*, 2012, **157**, 89–93.

61 F. Drache, V. Bon, I. Senkovska, C. Marschelke, A. Synytska and S. Kaskel, *Inorg. Chem.*, 2016, **55**, 7206–7213.

62 T. Loiseau, C. Serre, C. Huguenard, G. Fink, F. Taulelle, M. Henry, T. Bataille and G. Férey, *Chem. – Eur. J.*, 2004, **10**, 1373–1382.

63 H. Reinsch, M. A. van der Veen, B. Gil, B. Marszalek, T. Verbiest, D. de Vos and N. Stock, *Chem. Mater.*, 2013, **25**, 17–26.

64 E. Alvarez, N. Guillou, C. Martineau, B. Bueken, B. van de Voorde, C. Le Guillouzer, P. Fabry, F. Nouar, F. Taulelle, D. de Vos, J.-S. Chang, K. H. Cho, N. Ramsahye, T. Devic, M. Daturi, G. Maurin and C. Serre, *Angew. Chem., Int. Ed.*, 2015, **54**, 3664–3668.

65 K. Brandenburg, *Diamond 4.5.3, Crystal and Molecular Structure Visualization*, Crystal Impact - K. Brandenburg & H. Putz GbR, Bonn, Germany, 2009.

66 M. Wahiduzzaman, D. Lenzen, G. Maurin, N. Stock and M. T. Wharmby, *Eur. J. Inorg. Chem.*, 2018, 3626–3632.